ELSEVIER

Geomorphology 13 (1995) 215–232

GEOMORPHOLOGY

Spatial patterns of hydrology, geomorphology, and vegetation on the floodplain of the Amazon River in Brazil from a remote sensing perspective

Leal A.K. Mertes [a], Darin L. Daniel [a], John M. Melack [b], Bruce Nelson [c], Luiz A. Martinelli [d], Bruce R. Forsberg [e]

[a] *Department of Geography, University of California, Santa Barbara, CA 93106, USA*
[b] *Department of Biological Sciences, University of California, Santa Barbara, CA 93106, USA*
[c] *Department of Botany, Instituto Nacional de Pesquisas da Amazônia, Manaus, AM, Brazil*
[d] *Centro de Energia Nuclear na Agricultura, 13400 Piracicaba, SP, Brazil*
[e] *Department of Ecology, Instituto Nacional de Pesquisas da Amazônia, Manaus, AM, Brazil*

Received 3 November 1994; accepted 17 April 1995

Abstract

The spatial heterogeneity of hydrology and vegetation during high-water periods in geomorphically distinct reaches of the Amazon River in Brazil was determined based on semivariance statistics. The spatial statistics were derived from three classified Landsat Thematic Mapper images representing upstream to downstream geomorphic characteristics. In the upstream river reach, scroll-bar topography on the floodplain tends to channelize floodwater into floodplain drainage channels, thus reducing the diversity of water types by reducing opportunities for mixing of flooding river water with locally derived floodplain water. The highest diversity of vegetation types is along floodplain drainage channels, while the rest of the floodplain has a more homogeneous cover. In the middle reach of the river the diversity of wetland classes as measured by semivariance is higher than both upstream and downstream, perhaps because of exposure to more water types and landforms. The diversity of water types is high, because flooding river water flows onto the floodplain as diffuse, non-channelized overbank flow, as well as through drainage channels. The non-channelized overbank flow readily mixes with locally derived floodplain water. Floodplain landforms available for colonization by vegetation include scroll bars, swales, lake shores, lake deltas, and floodplain drainage channels. In the downstream reach where the floodplain is wide, relatively flat, and covered with huge lakes, the floodplain supports a moderately heterogeneous mix of vegetation communities. Where landforms are similar, the spatial distribution of the vegetation is similar to that of the middle reach of the river. In the downstream reach flooded forest comprised only 37% of the wetland vegetation. In contrast, in both the upstream and middle reaches, over 70% of the wetland vegetation was flooded forest. Agricultural clearing of the floodplain is more common in downstream reaches and may account for the smaller percent of floodplain forest cover.

1. Introduction

The spatial and temporal patterns and rates of water, sediment, and nutrients transfer through the Amazon floodplain directly influence the geomorphology and biogeochemistry of the Amazon River (Richey, 1983; Forsberg et al., 1988; Richey et al., 1989; Engle and Melack, 1993; Mertes, 1994; Mertes et al., 1995; Lesack and Melack, 1995). Junk et al. (1989) described the "flood-pulse" as a moving littoral zone of ever-increasing inundation on the floodplain. This description only partially characterizes the patterns and rates

SSDI 0169-555X(95)00038-0

of water transfer of the Amazon floodplain due to the variety of pathways for water to enter the floodplain. Annual inundation of the floodplain is the result of the hydrology of different water types as they enter the floodplain, either directly from rainfall, over land off surrounding slopes, flooding of local tributaries, groundwater, or exchange with the main channel (Richey et al., 1989). The spatial and temporal patterns of the hydrology are in turn influenced by the topography, soils, and vegetation of the floodplain. The variation in the patterns of mixing of different water types is such that in some reaches the floodplain fills with water from local sources long before the mainstem river flow overtops its banks. In other reaches river water may overtop the banks and inundate a dry floodplain. The manner in which the flood pulse passes through the floodplain should result in variability in the vegetation communities of the wetlands, given that several studies of Amazon wetland environments show succession, adaptation, and zonation of species influenced by hydroperiod (duration of inundation), degree of disturbance (e.g., deforestation, channel migration), and water chemistry (Worbes et al., 1992; Worbes, 1985; Lamotte, 1990; Kalliola et al., 1991, 1992; Campbell et al., 1992; Salo et al., 1986; Dumont et al., 1990; Parodi and Freitas, 1990).

Variation in spatial heterogeneity of the landscape is therefore expected on geomorphically and hydrologically distinct floodplains. Using semivariance statistics, we analyze the spatial relationship between the hydrogeomorphology and the pattern of vegetation cover of the Amazon River floodplain in Brazil during high water. Classified Landsat images for three reaches of the river that represent the geomorphology of the channel–floodplain system were analyzed to show the upstream to downstream variation in the spatial heterogeneity of the floodplain environments. In addition to hydrogeomorphic influence, in the downstream reaches vegetation heterogeneity appears to be impacted by human activities, in that flooded forest covers a smaller percent of the floodplain.

2. Background

Many wetlands studies have emphasized gaining a broad understanding of the relationships among hydroperiod, vegetation and wildlife communities (e.g., Bedinger, 1971; Leitman et al., 1984; Worbes, 1985; Keeland and Sharitz, 1992), and biogeochemistry (e.g., Devol et al., 1990; Maltby et al., 1992), and documenting average sedimentation rates (Hupp and Morris, 1990; Kleiss, 1992). Vegetation successional patterns associated with differently aged geomorphic surfaces (e.g., Sigafoos, 1961; Hupp and Osterkamp, 1985; Salo et al., 1986) illustrate the dynamic nature of riverine wetland templates. The topography, soil texture, and soil composition that characterize the physical template of wetlands are primarily controlled by channel migration and geomorphic processes active on the floodplain during inundation. However, the processes controlling the transfer of water between rivers and their associated wetlands and the transport of materials in the inundated sites are not well understood.

Investigation of the relation between hydrogeomorphology and vegetation communities has a long history on both temperate rivers (e.g., Sigafoos, 1961; Bedinger, 1971; Yanosky, 1982; Osterkamp and Hupp, 1984; Leitman et al., 1984; Hupp and Osterkamp, 1985; Brinson, 1993) and tropical rivers (e.g., Prance, 1979; Junk, 1984, 1989; Worbes, 1985; Klinge et al., 1990). For the Peruvian Amazon the debate has centered on whether the diversity of the forested wetlands is greater than the diversity of upland forests because of river dynamics (Salo et al., 1986; Kalliola et al., 1992) or whether the upland forests are more diverse due to relatively stable conditions compared to wetland forests (Dumont et al., 1990). In contrast, in the Brazilian Amazon the emphasis has been to determine the species and community relations to age patterns which in part determine the successional stages present (Worbes et al., 1992) or the impact of hydroperiod (Worbes, 1985) and sedimentation rates (Campbell et al., 1992) on species distribution and survival.

To use vegetation patterns to infer floodplain hydrology or the reverse requires knowledge of the seasonal and long-term patterns of inundation. There are a few field studies on the hydrology and hydraulics of floodplain flows (Wolman and Leopold, 1957; Popov and Gavrin, 1970; Velikanova and Yarnykh, 1970; Hughes, 1978; Lewin and Hughes, 1980; Mertes, 1990, 1994; Lesack and Melack, 1995). Hughes (1978, 1980) and Lewin and Hughes (1980) analyzed the relationship between the hydrology of a generic flood and the transfer of water between a channel and floodplain. They concluded that there will be a hysteresis in the relation-

ship between the change in the stage of a flood and the area of inundated floodplain, in that a floodplain typically will drain more slowly than fill, regardless of the rate of stage change. In addition, they suggested that the rate of rise and fall of the flood controls the size of the inundated area. For instance, if flow in the channel rises and falls rapidly, then less of the floodplain will be inundated, because the water cannot travel to the far reaches of the floodplain before the flow begins to recede. In this case, even though a flood may have a larger discharge than another smaller and slower-rising flood, less of the floodplain may be inundated. Water input associated with rainfall and local drainages directly flowing onto the floodplain would complicate further the patterns suggested by Hughes (1978, 1980) and Lewin and Hughes (1980).

Given the potential for variation of flooding, water mixing, geomorphology, and vegetation it would be ideal to determine a set of pattern metrics (Hunsaker and Levine, 1995) that would define the scale of "patchiness" of these wetland landscapes such that the metrics could be used to infer hydrologic, geomorphic, and biogeochemical process. The emphasis of this paper is to determine the relationships between Amazon floodplain hydrogeomorphology and vegetation by analyzing the spatial heterogeneity of the floodplain landscape.

3. Study area

Wetlands on the alluvial floodplains of the Amazon River and tributaries in Brazil are believed to cover over 300,000 km^2 (Klinge et al., 1990). The alluvial deposits along just the mainstem Amazon River in Brazil cover approximately 92,000 km^2 (Sippel et al., 1992). In this paper we describe results derived from analysis of 3 Landsat images (Fig. 1) that each cover 900 km^2 and represent geomorphically distinct reaches of the river in Brazil (Mertes et al., 1995). The first image is near the Japurá River confluence (Reach J), the second is near the town of Manacapurú (Reach M), and the third is near the town of Óbidos (Reach T).

The Amazon River and floodplain in Brazil show an upstream to downstream trend in channel behavior and geomorphology (Mertes et al., 1995). Representative floodplain types include a wide, scroll-bar floodplain with long, narrow lakes in Reach J (Fig. 1), a narrow floodplain with both long, narrow lakes and more equant lakes in Reach M, and a floodplain with a smooth surface with huge, multi-input, shallow lakes in Reach T. Rates of channel migration are higher in the upstream reaches, about 1.5% of the channel area is reworked annually, than the downstream reaches, less than 1% of the channel area is reworked annually (Mertes et al., 1995).

The Amazon floodplain can also be divided into the várzea, which is flooded by sediment- and nutrient-rich water (white water), and igapó, which is flooded by sediment- and nutrient-poor water (black water) (Sioli, 1968). The floodplain vegetation generally consists of forest, grassland, and "floating meadows" (Junk, 1970, 1984; Sternberg, 1975) whose spatial distribution, until recently, was described based primarily on detailed field studies at a few locations. Corves and Place (1994) and Melack et al. (1994) described the distribution of general categories of wetland vegetation based on classification of Landsat data and field data for areas in the central Amazon.

3.1. Hydrology

The pattern of inundation of the mainstem floodplain and the degree to which the different water types intermingle on the floodplain varies with position along the channel as shown by water storage computations based on combining data on bank topography with results from a one-dimensional (Muskingum) flood routing of the Amazon floodwave (Richey et al., 1989; Dunne et al., 1995). Elevations of river banks (Fig. 2) measured relative to the low-water surface at several sites along the mainstem of the river (Mertes, 1990) show a gradual decrease in a downstream direction from 11 m or more in the upstream reaches to less than 8 m in the downstream reaches (Fig. 2). The maximum difference in stage (Fig. 2) also decreases in a downstream direction from 12 to 13 m at upstream gages to 7.5 m at the furthest downstream gage at Óbidos.

Rates of overbank discharge per meter of bank length for the 1981 flood, with a recurrence interval of less than 5 years, are shown for the three reaches of the river (Fig. 3). The number of days of overbank discharge for this average flood are substantial, with 270 days in Reach J, 240 days in Reach M, and 156 days in Reach T. The later start to the floods downstream is primarily the result of the attenuation and diffusion of the flood-

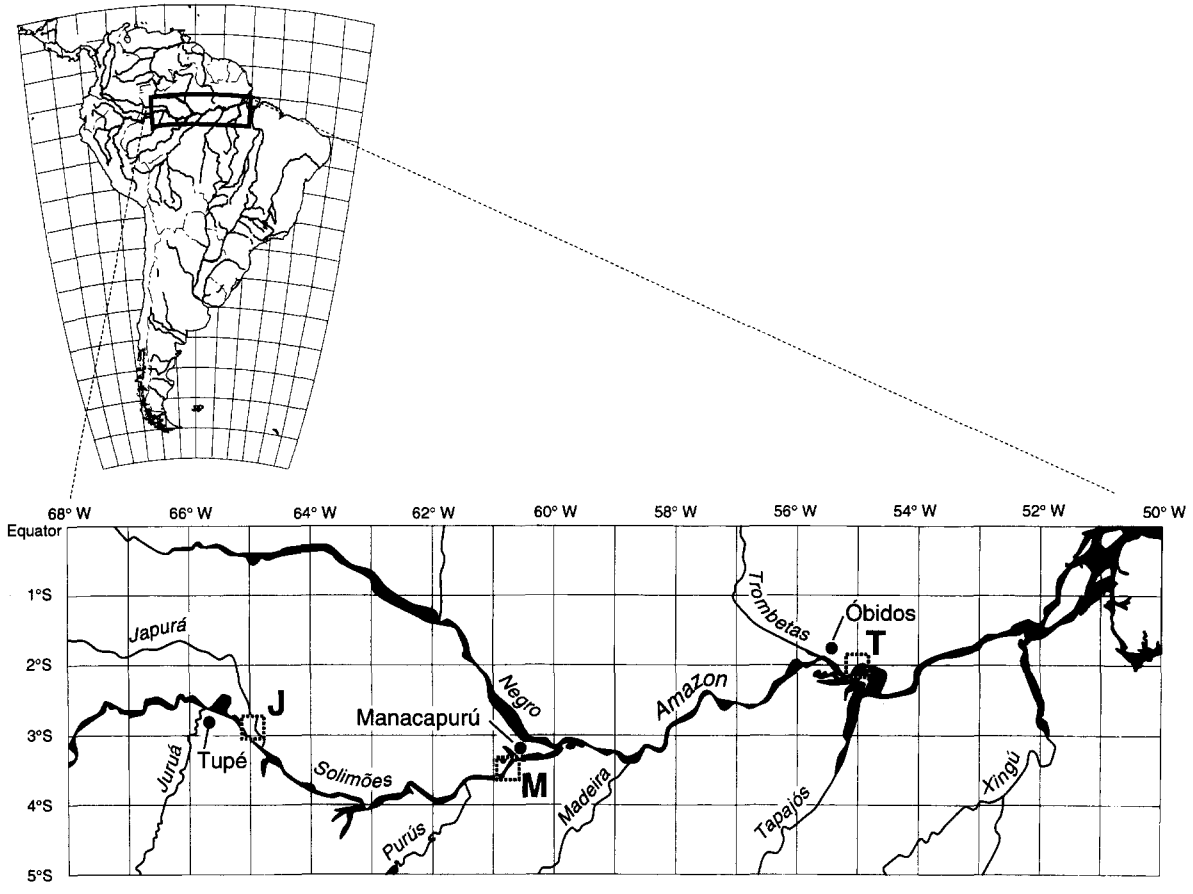

Fig. 1. Location map of the Amazon River in Brazil with the area outlined for each of the Landsat Thematic Mapper images described in this paper. J = Japurá Image, M = Manacapurú Image, and T = Tapajós Image.

wave which travels at an average rate of 0.3 m/s along the Brazilian reaches of the river (Richey et al., 1989).

The data shown in Fig. 3 indicate the rate of flooding assuming that all the water over-tops the bank once the channel is filled to capacity. However, mechanisms for flooding other than overbank flow are at work on the floodplain. For example, based on field data and two-dimensional numerical simulations of hydrology for Reach M, inundation appears to occur in three stages (Mertes, 1990). Initially, the floodplain begins to fill, at a river stage approximately 3 m above low water, as a result of a rising water table and water flowing through levee breaks associated with the deepest floodplain drainage channels. At this time the rate of filling directly by river water is minimal; less than 1% of the main channel discharge reaches the floodplain. However, lakes connected to the river by these deep drainage channels have nearly 100% mainstem water during this period of initial rise (Lesack and Melack, 1995). As the stage increases 4 to 7 m the numerous levee breaks associated with shallower floodplain channels are inundated, but the floodplain water still is comprised of local tributary, rain, or ground water. Finally, river water begins to enter the floodplain rapidly overbank once the stage exceeds approximately 10 m above the low-water level. A high correlation between the rise in stage and degree of inundation in this reach also was shown by Sippel et al. (1994) based on inundation area as determined from passive microwave data.

This three-stage inundation pattern is typical for the entire length of the river in Brazil and results in a nearly continuous net flow of water from the floodplain to the channel for all times of the year except during the middle part of the flood period (fig. 4 in Richey et al., 1989). One would expect that spatial and temporal variation in this three-stage pattern would be directly

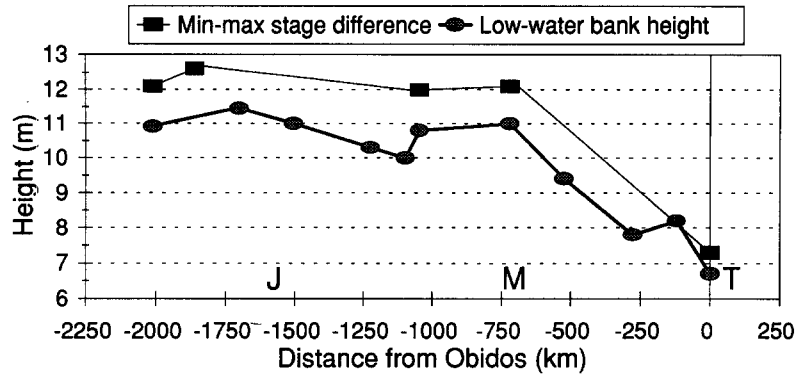

Fig. 2. Bank height with respect to low water based on topographic surveys of banks (Mertes, 1990) compared to the maximum difference between the lowest and highest river stage at mainstem gaging stations (hydrologic data from the Departamento Nacional de Aguas e Energia Elétrica).

related to the geomorphology of each reach as well as the hydrology. For example, in reaches where the banks are low and inundation is long, there is the greatest potential for exchange between the main channel and floodplain, and, hence, the greatest potential for mixing of the various types of water on the floodplain surface. In contrast, where local rainfall is substantial and precedes the flood crest, main channel waters can be blocked from entering the floodplain.

4. Landsat data

Three Landsat Thematic Mapper (TM) images (J, M, and T in Fig. 1) were made available through R. Almeida Filho of the Instituto Nacional Pesquisas Especiais (INPE). Image J was recorded on April 4, 1989 along Path 001/Row 062 with the center of the image at 2°54′S and 65°08′W. Image M was recorded on August 2, 1989 along Path 231/Row 062 with the center of the image at 2°54′ S and 60°34′ W. Image T is located at the confluence of the Amazon and Tapajós River, just downstream from the town of Óbidos which is the site for the last mainstem gaging station not influenced by tidal fluctuations. It was recorded on August 3, 1988 along Path 227/Row 62 with the center of the image at 2°54′S and 54°22′W.

Images were selected because the water levels were high and the floodplain was inundated. Approximate water discharges for the river for the time when these images were recorded (Fig. 4) include 80,700 m^3/s for Image J, 143,400 m^3/s for Image M, and 202,200 m^3/s at Óbidos for Image T (J. Richey, unpubl. data).

5. Methods

5.1. Spectral mixture analysis

A remotely sensed, multispectral image encodes information on atmosphere, lighting, and instrument conditions as well as information on the properties of surface materials. In addition to these potential inputs, every pixel may include information on a mixture of surface materials. In order to extract information regarding the surface materials, one must account for all of these distortions, which is possible using the technique of spectral mixture analysis (e.g., Smith et al., 1990). Briefly, spectral mixture analysis accounts for the pixel-by-pixel variation in the mixture composition by calculating the least-squares, best fit for each pixel along mixing lines bounded by spectra for endmembers. An endmember ideally represents a pure component of the mixtures present in the pixels of the image, e.g., soil or water. Previous applications of this technique to Landsat images of Amazon environments include Adams et al. (1990), Mertes et al. (1993), and Adams et al. (1995).

In this study spectral mixture analysis was used to determine the vegetation cover on the Amazon floodplain and the relative concentrations of suspended sediment in surface waters of the inundated floodplain. Bands 1 through 5 and 7 were used in all analyses, with an initial nominal calibration for path radiance by subtracting the minimum brightness value (DN) from each band. A complete calibration for atmospheric and instrument gains and offsets was not performed, because the analyses of these images was based on the

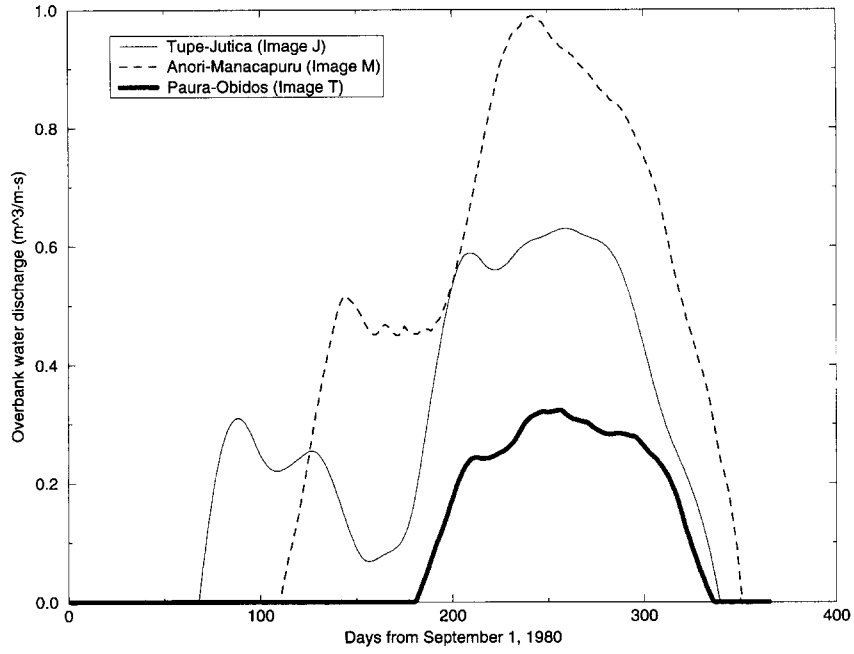

Fig. 3. Overbank water discharge for the 1981 water year (water year starts September 1). Data plotted for three reaches of the Amazon River located close to the areas recorded in the Landsat images. Method for calculation described by Dunne et al. (1995) and Richey et al. (1989).

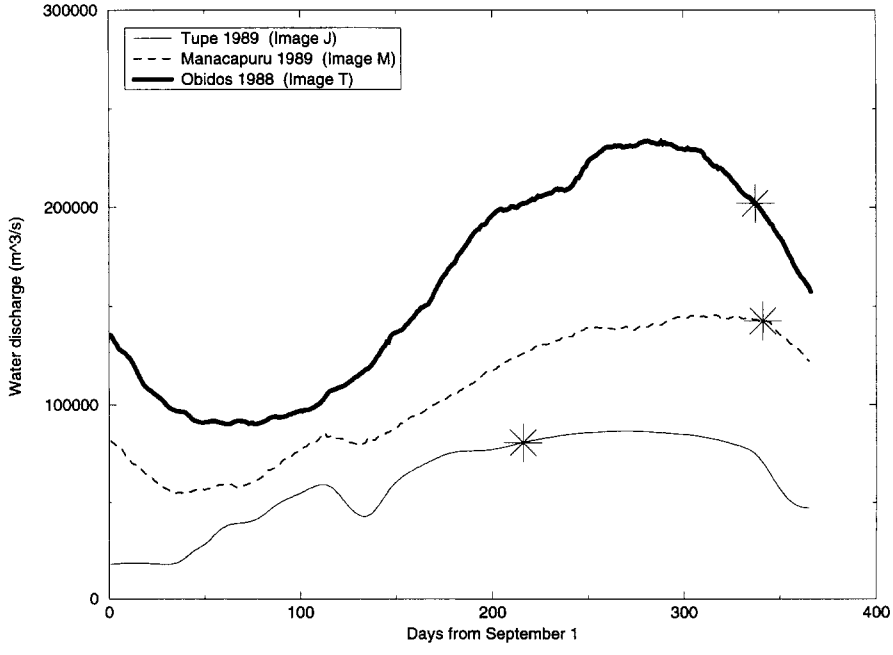

Fig. 4. Water discharge in main channel for three cross sections. Tupé hydrograph calculated from a Muskingum flood routing simulation (Richey et al., 1989). Manacapurú and Óbidos hydrographs developed from stage–discharge relations (J. Richey, unpubl. data) based on stage data from Departamento Nacional de Aguas e Energia Elétrica. Stars indicate date and water discharge when images were recorded in respective years.

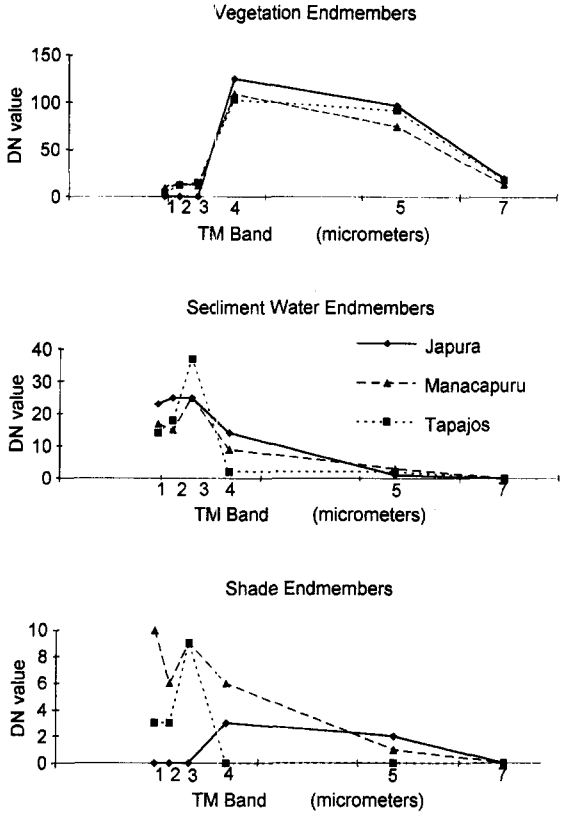

Fig. 5. Spectra for image endmembers selected from each Landsat TM scene for use in spectral mixture analysis.

distribution of the vegetation during just the time when the image was recorded and not across a temporal sequence of images. The spectral mixture analysis technique allows one to work with uncalibrated image data through the use of image endmembers.

For a multispectral image the image endmembers represent the purest sample of each component on the image. Image endmembers are similar to training data selected for use in other classification procedures such as maximum likelihood (Jensen, 1986), but differ in that ideally they represent one component of a landcover mixture like soil. Training data will often represent the entire mixture, e.g., forested wetland. For our analysis of the distribution of vegetation and sediment-laden water we selected three image endmembers for each image: vegetation, shade, and sediment–water (Fig. 5). The vegetation endmember was selected from pixels that show the most vigorous and dense vegetation growth. The shade endmember represents the darkest pixels and was always selected from deep, clear water bodies. Hence, the shade endmember provides information on the amount of both clear water and shade in a mixed pixel. The sediment–water endmember was selected from pixels that apparently had the highest sediment concentrations, which was always in the main channel. The sediment–water concentrations tend to be high enough to also represent some of the soils on the land surface.

Once these image endmembers were selected, they were used as input for a spectral mixture analysis, the result of which is a "fraction" image for each endmember. These fraction images show on a pixel-by-pixel basis the proportion (from 0 to 1.0) that is contributed by the spectra of the corresponding endmember. For example, a pixel from clear water would have fractions of 1.0 shade, 0 sediment water, and 0 vegetation. A pixel from a moderately dense, dry forest might have fractions of 0.2 shade, due to self-shading by leaves and branches (Roberts et al., 1990), 0.2 sediment water, due to reflectance from soil visible through the canopy, and 0.6 vegetation.

The fraction images can be viewed and interpreted individually or can be combined to provide an overall landcover classification from the processed image data (Adams et al., 1995). We passed the three fraction images for each Landsat scene (J, M, and T) through a parallelepiped classifier (Jensen, 1986) with thresholds that were set to distinguish four separate vegetation groups, five sediment–water groups, and five shade groups. For the vegetation the fractions ranged from -0.2 to 0.25, 0.26 to 0.50, 0.51 to 0.75, 0.76 to 1.2 for the four groups. The sediment water groups ranged from -0.2 to 0.0, 0.1 to 0.25, 0.26 to 0.50, 0.51 to 0.75, 0.76 to 1.2. The shade groups were calculated as the difference between 1.0 and the sum of the vegetation and sediment–water fractions. This differencing step is appropriate in our analysis, because in the spectral mixture modelling we constrained the fractions to sum to 1.0. Using this combination of fractions we had the potential to identify 14 different classes, which was considered sufficient resolution to analyze spatial heterogeneity on the floodplain.

The modelling allowed for a 20% fraction overflow (>1.0) and fraction underflow (<0.0) to compensate for slight variations in atmospheric conditions across the uncalibrated image. Fraction overflow and underflow indicate that the image endmembers selected are not the purest examples of endmembers for the image.

With variable atmospheric conditions a pure endmember in one part of a scene may also be brighter or darker than the identical surface elsewhere, simply due to light scattering in the atmosphere.

After completing the parallelepiped separation of the fraction data into classes with specified combinations of fractions we viewed each image and compared them to ground data to determine the general categories of wetland vegetation. For Image J a sequence of aerial photographs was taken October 6, 1984 (when discharge in the main channel was 38,700 m^3/s) and for Image M a sequence of aerial photographs was taken August 14, 1989 (two weeks after the image was recorded). The floodplain features documented with aerial photographs on August 14, 1989 in the area of Image M were confirmed with ground surveys following the August 14 flight. We also compared all of the Landsat results qualitatively to the side-looking radar mosaics of the Radambrasil (1972) project. Because of the close timing of the acquisition of Image M and the corresponding aerial photographs, we used this image for testing the validity of our spectral mixture analysis. We could not complete a full accuracy assessment, because the aerial photography was at such oblique angles that it was not possible to register the photograph to the image. However, detailed viewing of the images and the aerial photographs allowed us to confidently determine the general characteristics of the vegetation classes.

5.2. *Spatial analysis*

Two different image sizes were analyzed for spatial information on class distribution: a large image of 1000 by 1000 pixels (30 by 30 km) and a smaller image, subsampled from the large image, with only 500 pixels (15 km) on each side totalling 250,000 pixels. The large image contained floodplain, main channel, and small areas of upland (*terra firme*) environments. The small image only contained floodplain environments.

The percent cover and areal cover were calculated from histograms for each of the six images for all of the classes present in the images.

Semivariograms were calculated for the three smaller images to measure the spatial scale of the heterogeneity of the classes in each image. Semivariograms measure the spatial variation in a regionalized variable (Woodcock et al., 1988a, b). This type of random variable has a known position in either space or time. The theory of regionalized variables provides a simple means of measuring the spatial dependence of such variables (Curran, 1988). The semivariogram is a function that relates semivariance to spatial separation.

The semivariogram statistics were calculated directly from the image data, and distances were initially assigned as between-pixel distances and converted to meters (30 m per pixel) after the computation was completed. Specifically, the semivariogram or $\gamma(h)$ is calculated as:

$$\gamma(h) = \frac{1}{2(n-h)} \sum_{i=1}^{n-h} [z(x_1) - z(x_i + h)]^2 \qquad (1)$$

where h is the lag (or distance) over which γ (semivariance) is measured, n is the number of observations used in the estimate of $\gamma(h)$, and z is the value of the variable of interest at spatial position x_i (Journal and Huijbregts, 1978). The maximum semivariance reached is the sill. The distance, h, at which the sill is reached is called the range. The range is related to the spatial dependency in the image. At distances beyond the range samples can be described as independent. The sill reflects the magnitude of the variability.

For spectral data $\gamma(h)$ typically estimates the variability of radiance as a function of spatial separation (Cohen et al., 1990). For our data $\gamma(h)$ estimates the variability of categorical classes that were assigned arbitrary numeric values. Therefore, the semivariance calculated is meaningful for a relative comparison among images with the same class categories.

6. Analysis of results

6.1. *Endmembers for spectral mixture analysis*

Fig. 5 shows the pseudospectra, i.e., brightness values per band, for the image endmembers that were selected for each image. As expected, vegetation is very bright (high DN) in the infrared (Band 4) and relatively dark in the visible bands (1, 2, and 3), suggesting vigorous vegetation growth (Jensen, 1986). The sediment–water endmembers are very bright in the visible bands due to the increased scattering of light by the sediment particles in the water (Mertes et al., 1993; Kirk, 1986). In contrast the signal drops rapidly in the

near infrared and infrared bands due to the high rate of energy absorption by the water (Kirk, 1986). The shade endmember represents both shade and clear water and comprises the darkest pixels on the images. The ordinate values for the shade endmembers are a tenth of the vegetation values and half of the values for the sediment–water endmembers. The relative changes in the DN's for each image endmember are physically reasonable, given the landcover types they represent.

6.2. Wetland classes

Our final group of classified wetland communities and their associated fractions are listed in Table 1, and Figs. 6–8 show the classified images. Five different categories of water types were distinguished, with varying amounts of sediment present in the water. The three classes with the lowest sediment–water fractions (−0.2 to 0.5) were grouped into one class named "low sediment water" (LSW). Although we did not absolutely calibrate the sediment concentrations to milligrams per liter (Mertes et al., 1993), the spatial pattern of these classes suggest that these LSW classes represent water that likely did not originate from overbank flow of the main channel, and is instead locally derived floodplain water. In contrast, two fraction groups with sediment–water fractions from 0.51 to 1.2 were combined into the "high sediment water" (HSW) class that probably represents water that originated in the main channel. In Image J (Fig. 6), the Japurá River which lies on the northeastern side of the image also provides sediment-laden water to the floodplain. In the Tapajós image (Fig. 8) the class with a sediment–water fraction from 0.26 to 0.5 was put into the HSW class representing river water instead of LSW representing local floodplain water. Suspended sediment concentrations in the river are lower in the downstream reaches (Meade, 1985; Richey et al., 1986), and hence the fraction breakpoint between river and local-floodplain water is estimated to be lower in this downstream reach.

We distinguished two forest types, a dense flooded forest (DFF) and a low density flooded forest (LDFF). In the wetland forests trees have several strategies and adaptations for surviving in many cases nearly 200 days of deep inundation (Worbes et al., 1992). Hence, the phenology is often a direct function of the hydrology. While investigating the anomalies in growth rings for trees in the area near Image M, Worbes (1985) found that the formation of the distinctive annual rings was directly influenced by the pattern of defoliation of the trees. The strategies vary seasonally by species, which can directly affect the spectral response. For example, fewer leaves on a tree mean that more bark and substratum will be exposed (Roberts et al., 1990; Adams et al., 1995). If a substantial portion of the forest defoliates during high flows, then overall the forest will appear spectrally as less vigorous vegetation, and will

Table 1
Classes from parallelepiped classification

Class symbol	Class color	Class description	Fractions		
			Vegetation	Sedwater	Shade
LSW	dark blue	water with low sediment concentrations	−0.2 to 0.25	−0.2 to 0.0	0.75 to 1.0
LSW	dark blue	water with low sediment concentrations	−0.2 to 0.25	0.1 to 0.25	0.5 to 1.0
LSW[a]	dark blue	water with low sediment concentrations	−0.2 to 0.25	0.26 to 0.5	0.25 to 0.75
HSW	cyan	water with high sediment concentrations	−0.2 to 0.25	0.51 to 0.75	0.0 to 0.5
HSW	cyan	water with high sediment concentrations	−0.2 to 0.25	0.76 to 1.2	0.0 to 0.25
DFF	magenta	dense flooded forest	0.26 to 0.5	−0.2 to 0.0	0.5 to 0.75
LDFF	maroon	low density flooded forest	0.26 to 0.5	0.1 to 0.25	0.25 to 0.75
SM	yellow	senescent macrophyte	0.26 to 0.5	0.26 to 0.5	0.0 to 0.5
M/TFF	light green	macrophyte/*terra firme* forest	0.51 to 0.75	−0.2 to 0.0	0.25 to 0.5
DM	dark green	dense macrophyte	0.51 to 0.75	−0.2 to 0.0	0.25 to 0.5
U	black	unclassified/farmland?	mixed groups		

[a]HSW on Tapajós image, see text.
The class symbol is an acronym for the class description. Class colors are colors shown on Figures 5, 6, 7 and 8. Last three columns list the spectral mixture analysis fractions that were combined in a parallelepiped classification to yield each class.

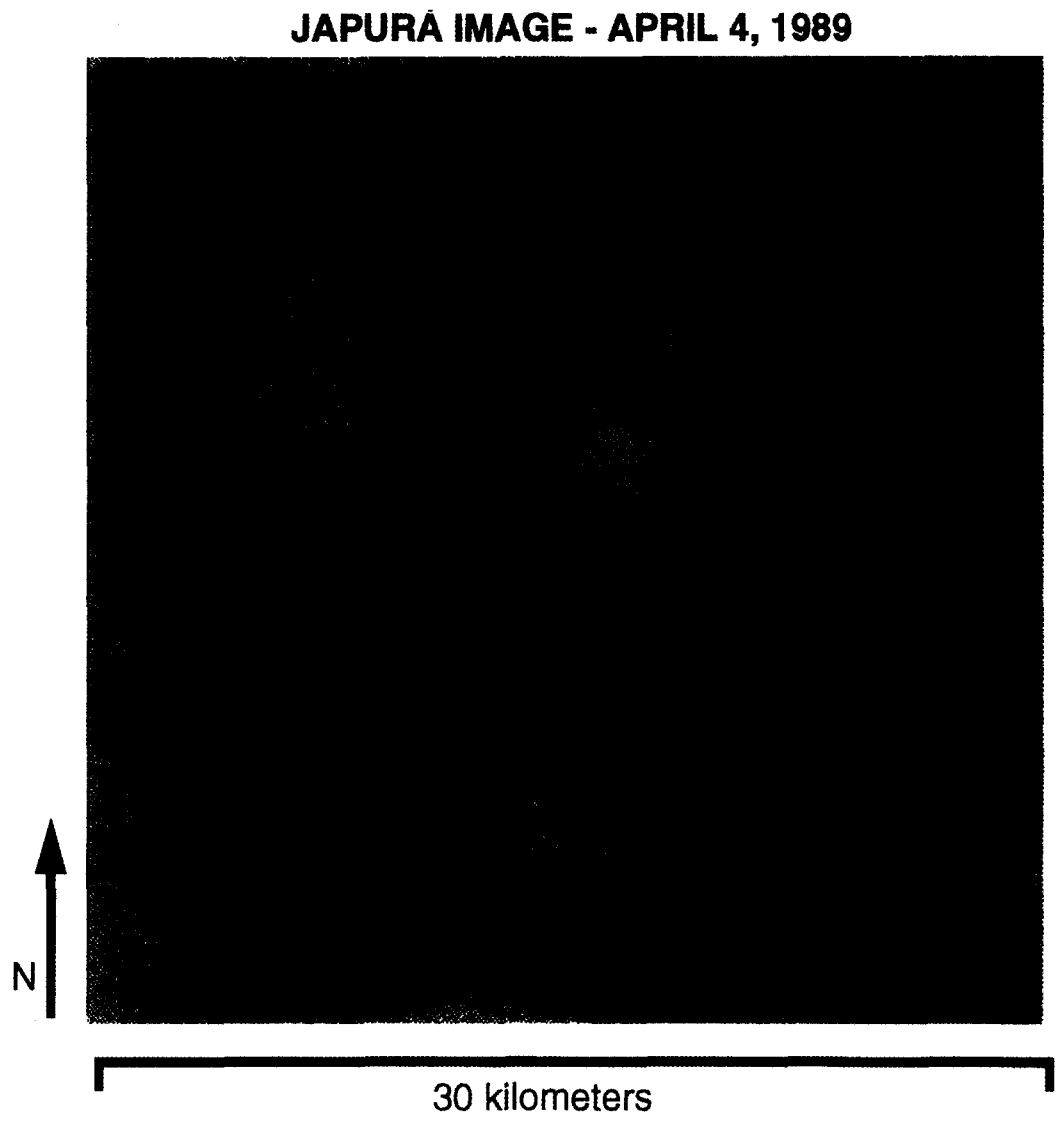

Fig. 6. Classified Landsat TM Image from the Japurá area (Image J) of the Amazon River and floodplain. Black outline shows location of subimage. Classes and corresponding colors are listed in Table 1.

show more spectral influence of the substratum, like flooding water. In our classification we characterized the dense flooded forest as having a 0.26 to 0.5 fraction of vegetation, essentially zero contribution from sediment–water, and a 0.5 to 0.75 shade fraction. We compared this category in detail for Image M with oblique aerial photographs and confirmed that the forested areas in this class appeared to have a more complete canopy cover than the LDFF class. The LDFF class had the same vegetation fractions, but a higher fraction of sediment–water, suggesting more substratum was exposed. Exposed bark may also account for the increase in the sediment–water fractions, because it has a similar spectrum to sediment or soils (Roberts et al., 1990). Evaluation of the aerial photographs showed that areas covered by the LDFF appeared to have lower and less dense canopies than the DFF.

Three categories of macrophytes were distinguished and their type confirmed on Image M based on comparing oblique aerial photographs. Macrophytes in general have relatively smooth surfaces with respect to light scattering, and therefore tend to return a much

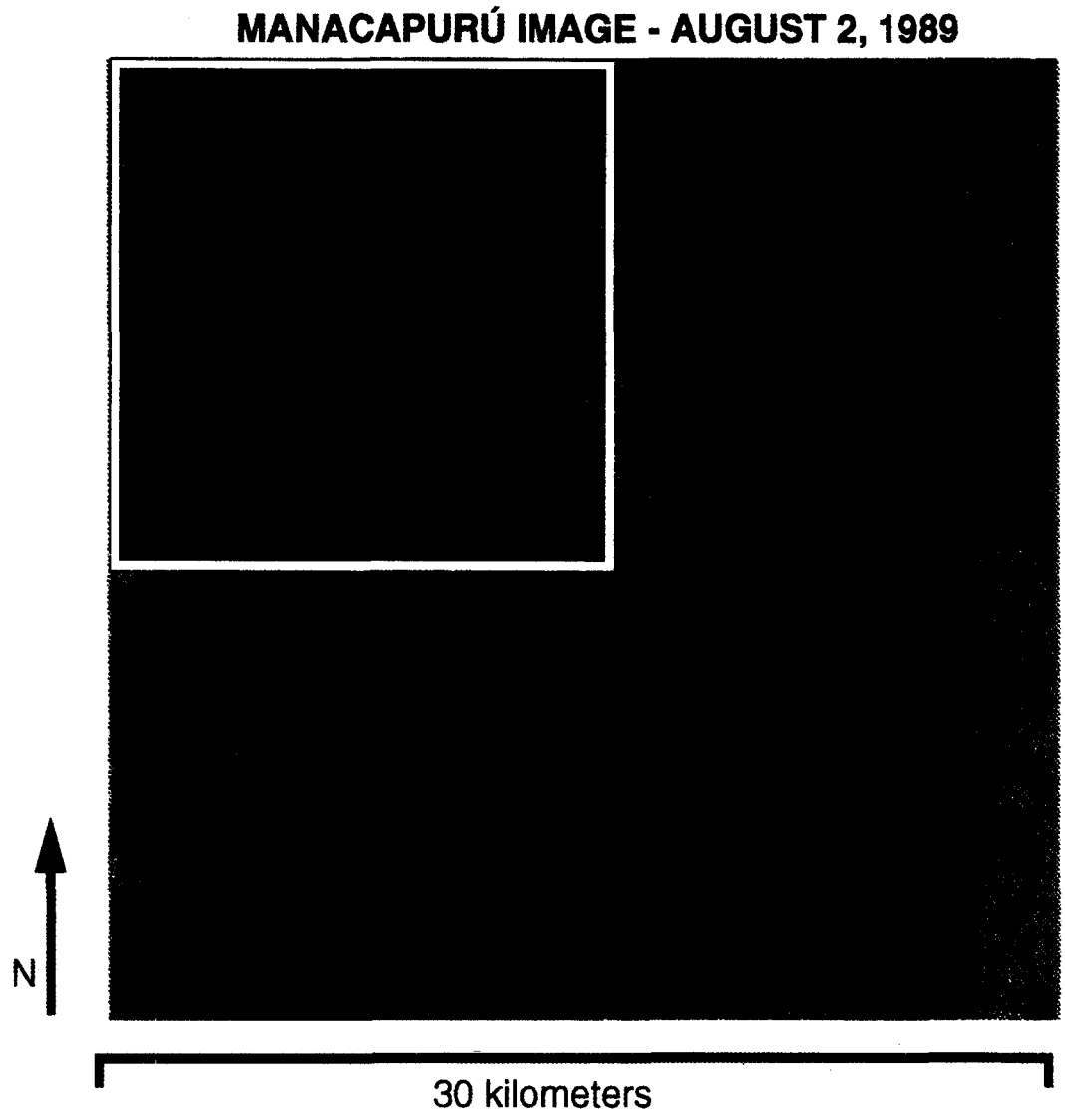

Fig. 7. Classified Landsat TM Image from the Manacapurú area (Image M) of the Amazon River and floodplain. White outline shows location of subimage. Classes and corresponding colors are listed in Table 1.

brighter signal than a tree canopy with complex limb structure and leaf self-shading. The dense macrophyte class (DM) had a very high vegetation fraction (0.76 to 1.2), a small amount of sediment–water (0.26 to 0.5) and no shade. This combination of fractions is a physically reasonable representation of a very dense, vigorously growing macrophyte bed. The less dense macrophytes (M) have a smaller vegetation fraction, with a slight increase in shade or clear water patches. This class also shows up in the *terra firme* forest, which is reasonable given that, in contrast to the floodplain forests, the *terra firme* forest typically has more dense vegetation cover and a higher degree of self-shading (Adams et al., 1995). The third macrophyte class has a smaller vegetation fraction (0.26 to 0.5), higher sediment–water fraction (0.26 to 0.5), and variable amounts of shade. We identified these areas as senesced macrophytes with variable proportions of green and brown vegetation. Again, the browned vegetation would have spectral properties similar to the sediment–water endmember. The spatial pattern of the senesced macrophytes also corresponds to the expected location

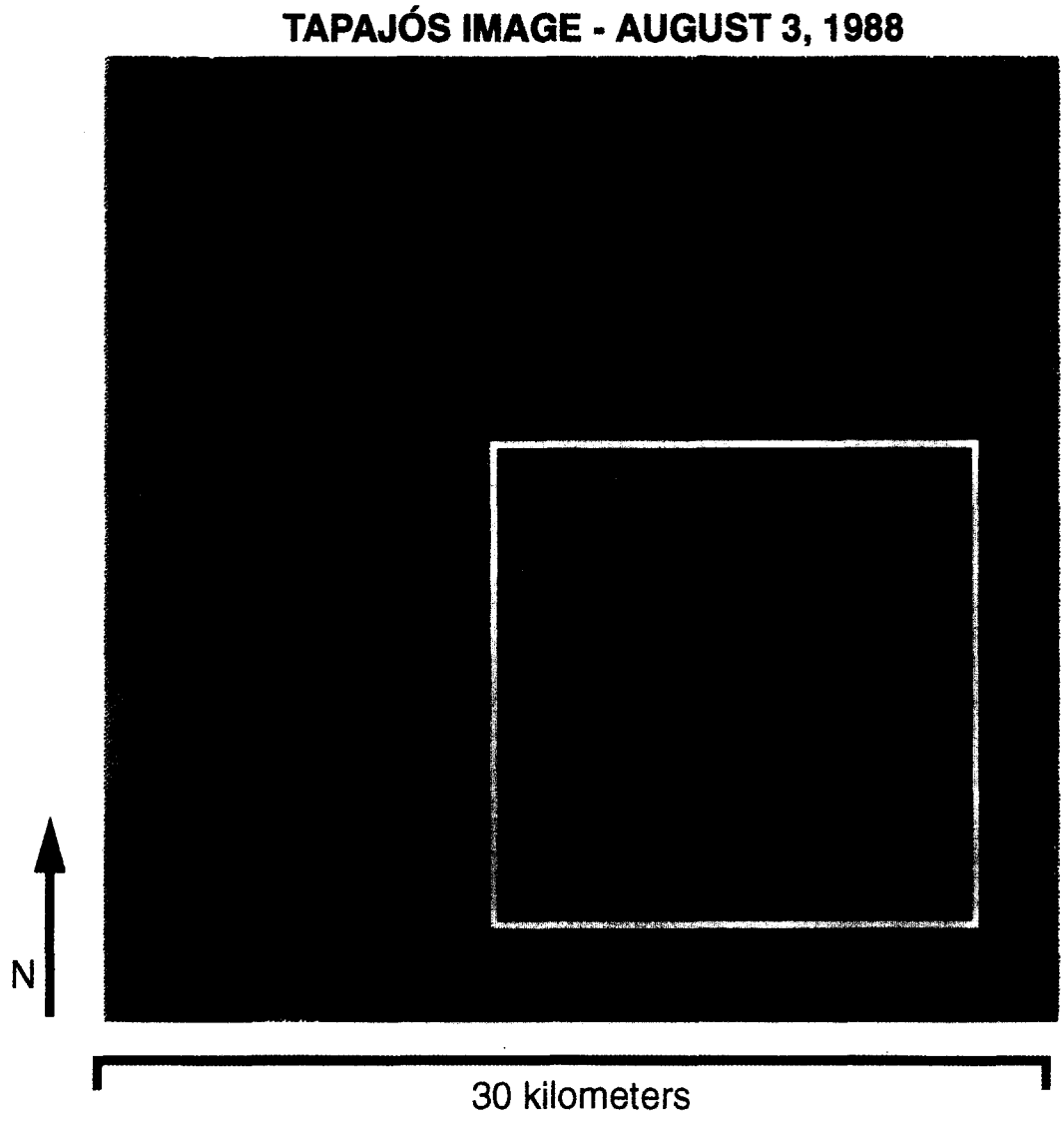

Fig. 8. Classified Landsat TM Image from the Tapajós area (Image T) of the Amazon River and floodplain. White outline shows location of subimage. Classes and corresponding colors are listed in Table 1.

of floating mats of dead grasses. They tended to be located in zones of poor water circulation, such as blocked channels.

6.3. Spatial analysis

Figs. 6–8 show that the spatial distribution of all of the classes varies from upstream to downstream.

When considering the spatial relation between hydrology and geomorphology, one way to track the pathways of water flow on the floodplain is to look for the regions that receive main channel floodwater. For Image J we estimated that the sediment-laden water of the main channel crossed a maximum of 5 km of the floodplain measured perpendicular to the main channel during this relatively high water period (Fig. 4). In addition, the only places on the floodplain where substantial flow of sediment-rich water existed was through the floodplain drainage channels that cross the floodplain surface (Fig. 6). Almost all of the other open water bodies were classified as LSW. In contrast, in Image M and Image T the water of the main channel

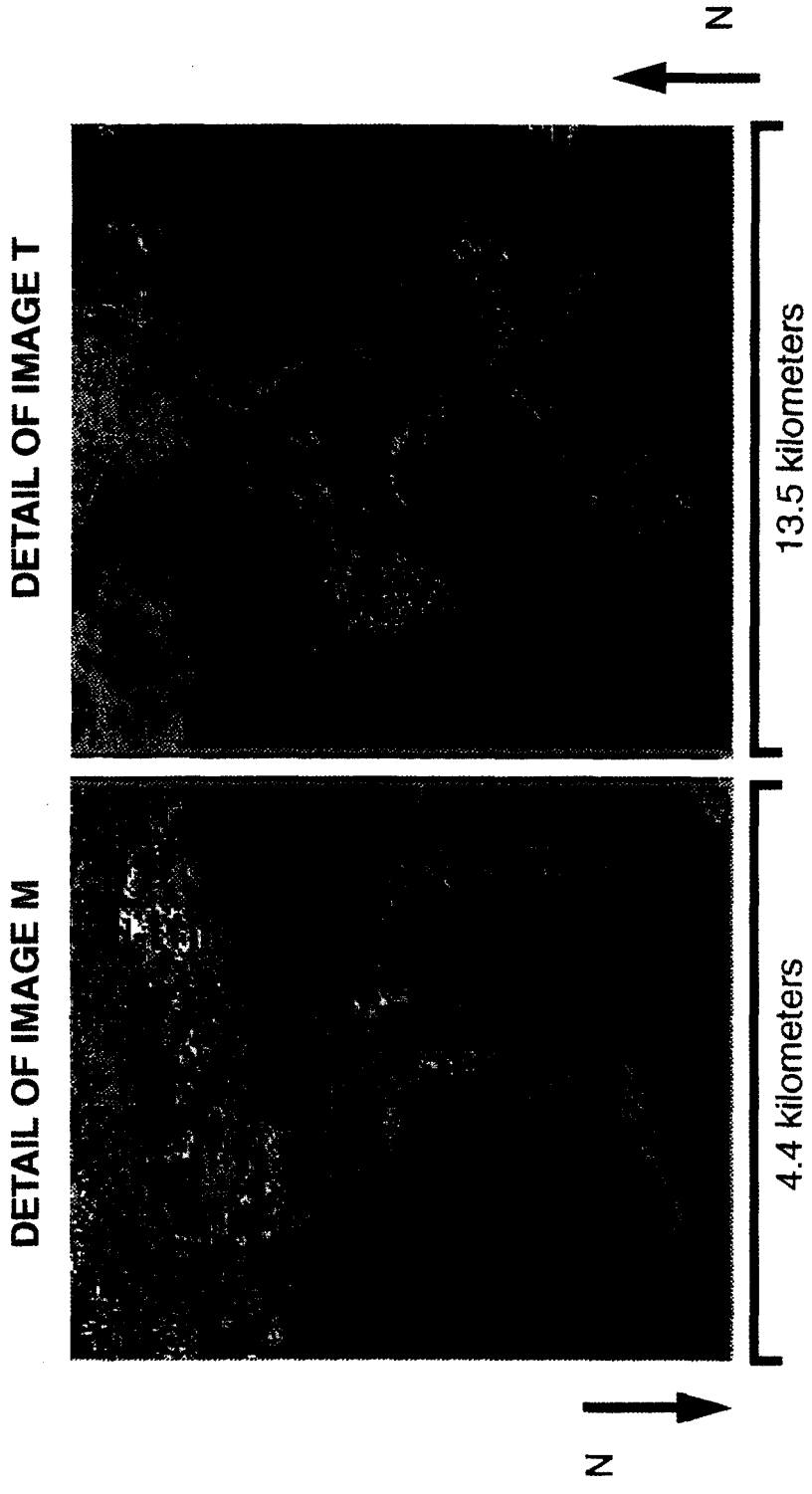

Fig. 9. Detailed view of sedimentary jetties (lake deltas) observed in Figs. 7 and 8. Classes and corresponding colors are listed in Table 1.

Table 2
Percent and areal cover for classes

Class	Japurá image		Manacapurú image		Tapajós image	
	Large	Small	Large	Small	Large	Small
Water types						
LSW	17 (155)	14 (31)	39 (352)	63 (141)	54 (485)	75 (168)
HSW	10 (94)	0.3 (0.7)	19 (171)	0.7 (2)	28 (252)	4 (9)
Floodplain forest types						
DFF	41 (370)	61 (137)	6 (50)	3 (8)	2 (23)	3 (7)
LDFF	4 (32)	3 (8)	8 (76)	10 (24)	5 (43)	4 (8)
Macrophytes						
DM	0.3 (2.7)	0.1 (0.3)	4 (34)	6 (14)	0.4 (4)	0.3 (0.7)
M/TFF	~14/~7 (~130/~70)	19/0 (44/0)	16/0 (140/0)	10/0 (22/0)	8/0 (77/0)	12/0 (28/0)
U	5 (41)	2 (4)	5 (44)	3 (7)	0	0

The percent cover and areal cover in square kilometers (in parentheses) for the different classes are listed for each river reach based on an analysis of two images —a large image comprised of one million pixels (900 km^2) and a small image comprised of 250,000 pixels (225 km^2) that was subsampled from the larger image to include only floodplain environments, i.e., no mainstem environments. No unclassified pixels were observed on the Tapajós image.

appears to have more diffuse access to the floodplain and travels an average distance of 15 km into the floodplain on Image M, and 20 km into the floodplain on Image T. In addition, in both Image M and T, open water bodies have some flow of sediment-laden water from the main channel. In particular, the detail in Fig. 9 shows two "sedimentary jetties" (usage Bird, 1964 as described by Blake and Ollier, 1971) where sediment from muddy river water is gradually building a deltalike feature at the edge of the lake. The delta channels provide additional flow paths for water from the main channel to enter large lakes during main channel floods.

In all three images the largest bodies of water that were classified as LSW are lakes with large local drain-

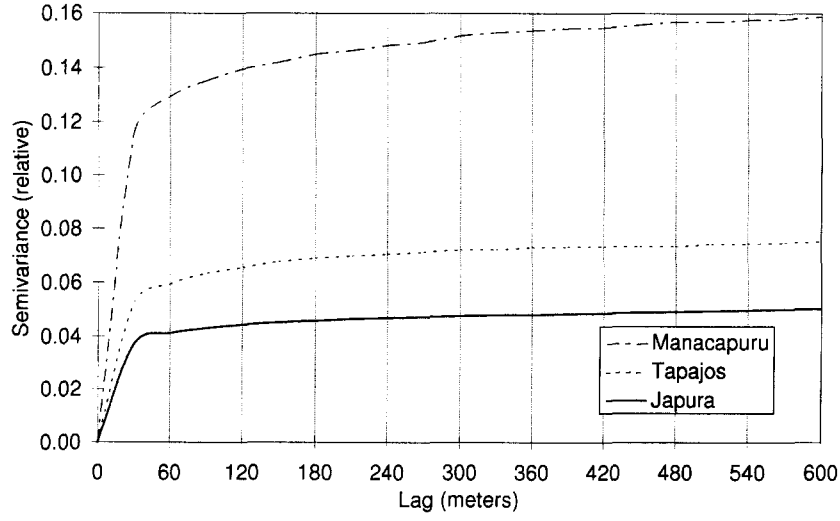

Fig. 10. Semivariogram for subimages of the three Landsat TM scenes shown in Figs. 6, 7, and 8. The meter scale on the abscissa represents the spatial scale of the variance shown on the ordinate. Semivariance values should be considered in a relative sense, as they are based on analysis of categorical classes with arbitrary numeric values.

ages. In Image J, Tefé Lake lies in the southwestern corner of the image (Fig. 6). The northwestern corner of Image M is dominated by the Cabaliana Lake complex (Fig. 7). The Tapajós River and mouthbay cover the entire bottom half of Image T (Fig. 8). As described by Forsberg et al. (1988), for lakes connected to the main channel through floodplain drainage channels, the ratio of local drainage basin area to lake area controls the relative proportions of local water and river water contributing to the lake on a seasonal basis. The larger the local drainage area, i.e., a ratio greater than 20, the less likely that river water incursion would significantly influence the lake hydrology. The three large lakes on these images all have very large drainage areas contributing flow. Hence, incursion of river water may occur but is not significant, or is typically channelized in a sedimentary jetty during high flow periods such as recorded in these images.

Summary statistics for the percent cover and areal cover for each wetland class are listed in Table 2. The primary difference between the large and small images is that the small images contain only floodplain environments. Therefore, it is not surprising that the largest differences between the class covers in all three images are the percents of the HSW class. In all three images, less main channel water of high sediment concentration was found on the smaller subimage. The relative proportion of the LSW water increased for Image M and T, because the small subimage still contained large areas of sediment-poor lake water, while the subimage for Image J was taken on the north bank of the river where the lakes are small.

Excluding HSW and LSW, the large and small images have a similar distribution of classes. The most abundant classes are DFF and M/TFF for Image J and M/TFF and LDFF for Images M and T. Excluding water cover (HSW and LSW) for each of the small images, the percentages for the largest classes are 72% of DFF for Image J, 40% of LDFF for Image M, and 62% of M/TFF for Image T. Of the total wetland vegetation cover, flooded forest comprises over 75% of both Image J and M, and less than 50% of Image T.

Percent cover does not provide information on the degree of heterogeneity or fragmentation of the landscape. Semivariance (γ) versus distance of separation or lag (h) is plotted for each of the subimages in Fig. 10. The curves show that the spatial scales of variation in all three images are similar. For example, all three images show some degree of variance at 30 m, the smallest lag considered due to the spatial resolution of the pixels. The differences among the images are that at each lag the semivariance is the smallest for Image J, second for Image T, and largest for Image M. Therefore, Image M has qualitatively higher heterogeneity of the wetland classes at all spatial scales than the other two images.

7. Discussion

Combining information on the hydrology, geomorphology, and vegetation of a floodplain environment makes it possible to identify the physical constraints that are the greatest influence on the transfer and storage of water, sediment, and other materials during inundation of the floodplain. Our analysis of three Landsat images selected to document high water periods in three geomorphically distinct reaches shows that there is a downstream variation in the hydrology, pattern of sediment transport, and spatial distribution of the vegetation. In the upstream reaches of the river the scroll-bar floodplain of Image J (Fig. 6) is typical (Mertes et al., 1995). As seen in Image J water flow onto the floodplain tends to be channelized. River water flows directly from the channel into lakes and floodplain areas at distances greater than 5 km, only by flowing through floodplain drainage channels. Given the fragmentation of the floodplain by the scroll-bar topography it is surprising that the vegetation distribution in Image J is relatively homogeneous. The most heterogeneous vegetation patterns are observed on islands in the main channel and along the boundaries of the floodplain drainage channels. It may be that the relative homogeneity of the rest of the floodplain surface is due to the fact that very little river water directly floods these areas, and the supply of nutrients and sediment is lower than near channels carrying river water. In addition, the environments are relatively stable because channel migration has probably not recently reworked the sites (Mertes et al., 1995). The vegetation communities therefore may be older and more homogeneous, similar to patterns described for western Amazonia (Salo et al., 1986).

Image M (Fig. 7) is located in the reaches of the river where the floodplain is typically narrow, has some scroll bars, and is covered by a mixture of long, narrow

lakes and small, rounder lakes (Mertes et al., 1995). The overbank flow of river water onto the floodplain is both channelized (center part of Image M) and non-channelized or diffuse (along both river banks). Both the lakes and drainage channels on the northern half of the floodplain appear to be filled with river water (HSW) and the general flow across the floodplain is from the southwest corner to the northeast corner. The spatial heterogeneity of the wetland classes is high, even at the smallest spatial separation of 30 m (Fig. 10). Finer resolution images may reveal that heterogeneity is high at even finer spatial scales. Corresponding aerial photographs and ground surveys show that the wetlands are indeed a complex mosaic of classes. This high heterogeneity suggests that the wetlands in this area might be exposed to a more diverse hydrology and mixing of water types (seasonal variations of local and river water mixing have been documented in this area, J. Melack, unpublished data), which may promote diversity. In addition, the types of landforms available for colonization by vegetation are more diverse in this section of the floodplain and include scroll bars, swales, lake shores, drainage channels, and lake deltas (Fig. 9). Each of these landforms would experience a slightly different inundation sequence of water flow, sediment transport, and nutrient supply, promoting greater vegetation diversity.

The wide floodplain near Image T (Fig. 8) generally has a surface with lower relief than upstream and is covered by huge, shallow, multi-input, round lakes (Mertes et al., 1995). As documented on Image T flow of water directly onto the floodplain from the main channel may be nonchannelized, channelized, or blocked by water flowing out of a large tributary. The longest pathway for incursion of river water, 20 km, into the large lake of the Tapajós River is along the sedimentary jetty (Fig. 9). Non-channelized flow into the large lake was not observed, unlike the nonchannelized flow of river water across the lakes in Image M. The spatial heterogeneity of the wetland classes of Image T is intermediate between Image J and Image M. When the wetlands are viewed in detail, it appears that the diversity of classes is highest on the lake delta (Fig. 9) and main channel islands, where the landforms are diverse and, in the case of the islands, relatively unstable (Mertes et al., 1995). The more homogeneous cover along the edge of the lake where only a small percent of floodplain forest is present, compared to higher percents in the same environments upstream, may in part be the result of land use practices in this area where agricultural clearing of the floodplain is common (Smith et al., 1991).

8. Conclusions

Two landscape metrics, percent cover and semivariance, were used to describe the spatial distribution and heterogeneity of wetland classes in representative reaches of the Amazon River and floodplain in Brazil. Three processed Landsat images representing the upstream to downstream character of the hydrology and geomorphology of the channel-floodplain system show unique spatial patterns of wetland classes. This type of landscape mapping provides insight into the physical processes controlling construction and maintenance of floodplain landforms and the growth of distinct vegetation communities. In turn, these unique associations of hydrology, geomorphology, and vegetation, as defined by the metrics, potentially provide information on patterns of nutrient utilization and the associated biogeochemistry of the wetland environments. Temporal and spatial variations in the spectral response resulting from seasonal changes in the phenology of the different forest species may result in seasonally different landscape metrics. Seasonal changes are being investigated with temporal sequences of images. Efforts to link landscape metrics to the hydrologic, geomorphic, vegetative, and biogeochemical character of the entire mainstem Amazon floodplain in Brazil are underway.

Acknowledgements

Many scientists contributed to the concepts developed in this paper including, Drs. J. Richey, T. Dunne, J. Adams, E. Novo, C. Hunsaker, E. Drago, and R. Meade. Images were made available by R. Almeida Filho of the Instituto Nacional Pesquisas Especiais (INPE) of Brazil. This work was supported by the National Science Foundation Grant DEB-9120038 and NASA Grant NAGW 2652. CAMREX contribution number 69. This paper is dedicated to the memory of Dr. Jeffrey L. Star.

References

Adams, J.B., Kapos, V., Smith, M.O., Filho, R.A., Gillespie, A.R. and Roberts, D.A., 1990. A new Landsat view of land use in Amazonia. Int. Symp. on Primary Data Acquisition, ISPRS, Manaus, 1990.

Adams, J.B., Sabol, D., Kapos, V., Filho, R.A., Roberts, D.A., Smith, M.O., and Gillespie, A.R., 1995. Classification of multispectral images based on fractions of endmembers: Application to land-cover in the Brazilian Amazon. Remote Sensing Environ., in press.

Bedinger, M.S., 1971. Forest species as indicators of flooding in the lower White River Valley, Arkansas. U.S. Geol. Surv. Prof. Pap., 750-C: C248–C253.

Bird, E.F.C., 1964. Coastal Land Forms. Australian National University, Canberra.

Blake, D.H. and Ollier, C.D., 1971. Alluvial plains of the Fly River, Papua. Z. Geomorphol. N.F. Suppl., 12: 1–17.

Brinson, M.M., 1993. Changes in the functioning of wetlands along environmental gradients. Wetlands, 13: 65–74.

Campbell, D.G., Stone, J.L. and Rosas, A., Jr., 1992. A comparison of the phytosociology and dynamics of three floodplain (Várzea) forests of known ages, Rio Juruá, western Brazilian Amazon. Bot. J. Linnean Soc., 108: 213–237.

Cohen, W.B., Spies, T.A. and Bradshaw, G.A., 1990. Semivariograms of digital imagery for analysis of conifer canopy structure. Remote Sensing Environ., 34: 167–178.

Corves, C. and Place, C.J., 1994. Mapping the reliability of satellite-derived landcover maps — an example from the Central Brazilian Amazon Basin. Int. J. Remote Sensing, 15: 1283–1294.

Curran, P.J., 1988. The semivariogram in remote sensing: An Introduction. Remote Sensing Environ., 24: 493–507.

Devol, A.H., Richey, J.E., Forsberg, B.R. and Martinelli, L.A., 1990, Seasonal dynamics in methane emissions from the Amazon River floodplain to the troposphere. J. Geophys. Res. — Atmospheres 95/ND10: 16417–16426.

Dumont, J.F., Lamotte, S. and Kahn, F., 1990. Wetland and upland forest ecosystems in Peruvian Amazonia: Plant species diversity in the light of some geological and botanical evidence. For. Ecol. Manage., 33/35: 125–139.

Dunne, T., Mertes, L.A.K., Meade, R.H. and Richey, J.E., 1995. Sediment transport and sedimentation along the Solimões–Amazon River, Brazil. Geol. Soc. Am. Bull., submitted.

Engle, D.L. and Melack, J.M., 1993. Consequences of riverine flooding for seston and the periphyton of floating meadows in an Amazon floodplain lake. Limnol. Oceanogr., 38: 1500–1520.

Forsberg, B.R., Devol, A.H., Richey, J.E., Martinelli, L.A. and Dos Santos, H., 1988, Factors controlling nutrient concentrations in Amazon floodplain lakes. Limnol. Oceanogr., 33: 41–56.

Hughes, D.A., 1978. Flooding and floodplain inundation (Ph.D. Thesis). University College of Wales, Aberystwyth, 252 pp.

Hughes, D.A., 1980. Floodplain inundation: Processes and relationships with channel discharge. Earth Surf. Process., 5: 297–304.

Hunsaker, C.T. and Levine, D.A., 1995. Hierarchical approaches to the study of water quality in rivers. BioScience, 45: 193–203.

Hupp, C.R. and Morris, E.E., 1990. A dendrogeomorphic approach to measurement of sedimentation in a forested wetland, Black Swamp, Arkansas. Wetlands, 10: 107–124.

Hupp, C.R. and Osterkamp, W.R., 1985. Bottomland vegetation distribution along Passage Creek, Virginia, in relation to fluvial landforms. Ecology, 66: 670–681.

Jensen, J.R., 1986. Introductory Digital Image Processing. Prentice-Hall, Englewood Cliffs, N.J., 379 pp.

Journal, A.G. and Huijbregts, C.J., 1978. Mining Geostatistics. Academic Press, New York.

Junk, W.J., 1970. Investigations on the ecology and production biology of the floating meadows (*Paspalo–Echinochloetum*) on the Middle Amazon, Part 1: the floating vegetation and its ecology. Amazoniana, 2: 449–495.

Junk, W.J., 1984. Ecology of the várzea, floodplain of Amazonian whitewater rivers. In: H. Sioli (Editor), The Amazon. Junk, Dordrecht, pp. 215–243.

Junk, W.J., 1989. Flood tolerance and tree distribution in Amazonian floodplains. In: L.B. Nielsen, I.C. Nielsen and H. Balslev (Editors), Tropical Forests: Botanical Dynamics, Speciation, and Diversity. Academic Press, London, pp. 47–64.

Junk, W.J., Bayley, P.B. and Sparks, R.E., 1989. The flood pulse concept in river–floodplain systems. In: D.P. Doge (Editor), Proc. Int. Large River Symp. Can. Fish. Aquat. Sci. Spec. Publ., 106: 110–127.

Kalliola, R., Salo, J., Puhakka, M. and Rajasilta, M., 1991. New site formation and colonizing vegetation in primary succession on the western Amazon floodplains. J. Ecol., 79: 877–901.

Kalliola, R., Salo, J., Puhakka, M., Rajasilta, M., Häme, T., Neller, R.J., Räsänen, M.E. and Dan-joy Arias, W.A., 1992. Upper Amazon channel migration. Naturwissenschaften, 79: 75–79.

Keeland, B.D. and Sharitz, R.R., 1992. The effects of fluctuating hydrologic regimes on the growth of three wetland tree species [abs]. INTECOL — IV International Wetlands Conference, Columbus, September 13–18, p. 61.

Kirk, J.T.O., 1986. Light and Photosynthesis in Aquatic Ecosystems. Cambridge University Press, Cambridge, 401 pp.

Kleiss, B.A., 1992. Methods for measuring sedimentation rates in bottomoland hardwood wetlands. Wetlands Research Program Technical Note: SD-CP-4.1, USAE Waterways Experiments Station, Vicksburg, MS.

Klinge, H., Junk, W.J. and Revilla, C.J., 1990. Status and distribution of forested wetlands in tropical South America. For. Ecol. Manage., 33/34: 81–101.

Lamotte, S., 1990. Fluvial dynamics and succession in the lower Ucayali River basin, Peruvian Amazon. For. Ecol. Manage., 33/34: 141–156.

Leitman, H.M., Sohm, J.E. and Franklin, M.A., 1984. Wetland hydrology and tree distribution of the Apalachicola River flood plain, Florida. U.S.G.S. Water-Supply Pap., 2196: 52 pp.

Lesack, L.F.W. and Melack, J.M., 1995, Flooding hydrology and mixture dynamics of lake water derived from multiple sources in an Amazon floodplain lake. Water Resour. Res., 31: 329–346.

Lewin, J. and Hughes, D., 1980. Welsh floodplain studies II. Application of a qualitative inundation model. J. Hydrol., 46: 35–49.

Maltby, E., Van der Peijl, M., Hoga, D. and Immirxi, C.P., 1992. Building a new approach to the investigation and assesment of

wetland ecosystem functioning [abs.]. INTECOL — IV International Wetlands Conference, Columbus, September 13–18, p. 47.

Melack, J.M., Hess, L.L. and Sippel, S., 1994. Remote sensing of lakes and floodplains in the Amazon Basin. Remote Sensing Rev., 10: 127–142.

Meade, R.H., 1985. Suspended sediment in the Amazon River and its tributaries in Brazil during 1982–1984. U.S. Geol. Surv. Pap., 85-492: 39 pp.

Mertes, L.A.K., 1990. Hydrology, hydraulics, sediment transport, and geomorphology of the central Amazon floodplain. Ph.D. Thesis. University of Washington, Seattle, 225 pp.

Mertes, L.A.K., 1994, Rates of flood-plain sedimentation on the central Amazon River. Geology, 22: 171–174.

Mertes, L.A.K., Smith, M.O. and Adams, J.B., 1993. Estimating suspended sediment concentrations in surface waters of the Amazon River wetlands from Landsat images. Remote Sensing Environ., 43: 281–301.

Mertes, L.A.K., Dunne, T. and Martinelli, L.A., 1995. Channel-floodplain geomorphology along the Solimões–Amazon River, Brazil. Geol. Soc. Am. Bull., submitted.

Osterkamp, W.R. and Hupp, C.R., 1984. Geomorphic and vegetative characteristics along three northern Virginia streams. Geol. Soc. Am. Bull., 95: 1093–1101.

Parodi, J.L. and Freitas, D., 1990. Geographical aspects of forested wetlands in the lower Ucayali, Peruvian Amazon. For. Ecol. Manage., 33/34: 157–168.

Popov, I.V. and Gavrin, Y.S., 1970. Use of aerial photography in evaluating the flooding and emptying of river flood plains and the development of flood plain currents. Sov. Hydrol. Selected Pap., 5: 413–425.

Prance, G.T., 1979. Notes on the vegetation of Amazonia III. The terminology of Amazonian forest types subject to inundation. Brittonia, 31: 26–38.

Radambrasil, 1972. Mosaico semi-contralado de radar. Ministerio das Minas e Energia Departamento Nacional de Producão Mineral, Rio de Janeiro, scale 1:250,000.

Richey, J.E., 1983. Interaction of C, N, P, and S in river systems: a biogeochemical model. In: B. Bolin and R.B. Cook (Editors), The Major Biogeochemical Cycles and Their Interactions. Wiley, New York, pp. 365–383.

Richey, J.E., Meade, R.H., Salati, E., Devol, A.H., Nordin, C.F., Jr. and Santos, U. deM., 1986. Water discharge and suspended sediment concentrations in the Amazon River, 1982–1984. Water Resour. Res., 22: 756–764.

Richey, J.E., Mertes, L.A.K., Dunne, T., Victoria, R.L., Forsberg, B.R., Tancredi, A. and Oliveira, E., 1989. Sources and routing of the Amazon River flood wave. Global Biogeochem. Cycles, 3: 191–204.

Roberts, D.A., Adams, J.B. and Smith, M.O., 1990. Transmission and scattering of light by leaves: effects on spectral mixtures. Proc. Int. Geosciences Remote Sensing Symp., 2: 1381–1385.

Salo, J., Kalliola, R., Häkkinen, I., Mäkinen, Y., Niemalä, P., Puhakka, M. and Coley, P.D., 1986. River dynamics and the diversity of Amazon lowland forest. Nature, 322: 254–258.

Sigafoos, R.S., 1961. Vegetation in relation to flood frequency near Washington, D.C. U.S. Geol. Surv. Prof. Pap., 424-C: 248–250.

Sioli, H., 1968. Hydrochemistry and geology in the Brazilian Amazon region. Amazoniana, 1: 267–277.

Sippel, S.J., Hamilton, S.K. and Melack, J.M., 1992. Inundation area and morphometry of lakes on the Amazon River floodplain, Brazil. Arch. Hydrobiol., 123: 385–400.

Sippel, S.J., Hamilton, S.K., Melack, J.M. and Choudhury, B.J., 1994. Determination of inundation area in the Amazon River floodplain using the SMMR 37 GHz polarization difference. Remote Sensing Environ., 48: 70–76.

Smith, N.J.H., Alvim, P., Homma, A., Falesi, I. and Serrão, A., 1991. Environmental impacts of resource exploitation in Amazonia. Global Environ. Change, 1: 313–320.

Smith, M.O., Ustin, S.L., Adams, J.B. and Gillespie, A.R., 1990. Vegetation in deserts: I. A regional measure of abundance from multispectral images. Remote Sensing Environ., 31: 1–26.

Sternberg, H.O'R., 1975. The Amazon River of Brazil. Geogr. Z. Beih., 40: 74 pp.

Velikanova, Z.M. and Yarnykh, N.A., 1970. Field investigations of the hydraulics of a floodplain during a high flood. Sov. Hydrol. Selected Pap., 5: 33–53.

Wolman, M.G. and Leopold, L.B., 1957. River flood plains: some observations on their formation. U.S. Geol. Surv. Prof. Pap., 282-C: 81–107.

Woodcock, C.E., Strahler, A.H. and Jupp, D.L.B., 1988a. The use of variograms in remote sensing: I. Scene models and simulated images. Remote Sensing Environ., 25: 323–343.

Woodcock, C.E., Strahler, A.H. and Jupp, D.L.B., 1988b. The use of variograms in remote sensing: II. Real digital images. Remote Sensing Environ., 25: 349–379.

Worbes, M., 1985. Structural and other adaptations to long-term flooding by trees in Central Amazonia. Amazoniana, 3: 459–484.

Worbes, M., Klinge, H., Revilla, J.D. and Martius, C., 1992. On the dynamics, floristic subdivision and geographical distribution of várzea forests in Central Amazonia.

Yanosky, T.M., 1982. Effect of flooding upon woody vegetation along parts of the Potomac River flood plain. U.S. Geol. Surv. Prof. Pap., 1206: 21 pp.